Proceedings of AJCPP2012
Asian Joint Conference on Propulsion and Power
March 1-4, 2012, Xi'an, China

AJCPP2012-170

Aerodynamic Heating on Cowl Blunt Leading Edge of Hypersonic Inlet

Hongbo LU, Lianjie Yue, Yabin XIAO, Lihong CHEN, Xinyu CHANG
Key Laboratory of High Temperature Gas Dynamics, Institute of Mechanics, CAS
No.15 Beisihuanxi Road, Beijing 100190, China
luhongbo@imech.ac.cn

Keywords: hypersonic inlet, blunt cowl-lip, aerodynamic heating

Abstract

This Mach 6 study provides the first detailed pressure and heat transfer rate distributions from a two-dimensional compression wave interference pattern created by a noncoalesced isentropic wave intersecting the bow shock wave of a cylinder. The cylinder is representative of the cowl leading edge of a rectangular hypersonic engine inlet. Shock–interference-pattern, pressure and heat transfer rate which result from the noncoalesced isentropic compression wave intersecting the cowl bow shock directly relies on the ratio of the intersection portion length of the isentropic compression wave and the cowl shock to the strong part length of the cowl shock, that is to say $\overset{\frown}{CD} / \overset{\frown}{AB}$. When $\overset{\frown}{CD} / \overset{\frown}{AB}$ tends to zero order magnitude as well as a noncoalesced isentropic compression wave intersecting cowl bow shock, Type IV shock pattern occurs, and pressure, heat transfer rate dramatically amplifies. Otherwise, when $\overset{\frown}{CD} / \overset{\frown}{AB}$ draws near one order magnitude, shock-pattern does not exist and the amplification of pressure, heat transfer rate decreases with $\overset{\frown}{CD} / \overset{\frown}{AB}$ increasing.
.

Introduction

Scramjet is the key technology of hypersonic air-breathing vehicles. As a critical component of scramjet, hypersonic two-dimensional inlet generally employs a mixed-compression intake, which consists of the external and internal compression components, to compress the free-stream air. The external component is mostly composed of a wedge and an isentropic compression surface. In order to obtain good aerodynamic performance, the ideal inlet adopts a wedge and a sharp cowl-lip. However, the sharp ramp, cowl and other leading edges are easily burned because of the serious aerodynamic heating problem at hypersonic flight conditions[1)]. Considering the thermal protection, the sharp leading edge of the hypersonic inlet must be blunted properly. Also, a truly sharp edge would be impossible to manufacture.

For efficient operation, the external compression waves must intersect the engine cowl. This minimizes the spillage of compressed air outside the engine and prevents unwanted shock wave reflections inside the inlet. However, this condition will result in an interaction between the ramp shock or the isentropic compression wave and the bow shock around the cowl-lip. Many of the examples above involve a straight, oblique shock wave intersecting a bow shock[2-8)]. Edney[2)] characterized six interactions (Types I-VI) depending on the intersecting location of the incident oblique shock relative to the curved bow shock. Some refinements to these classifications have been made subsequently, but the basic six still demonstrate the range of phenomena observed, including shock wave / boundary layer interactions, expansion fan / boundary layer interactions, shear layer impingement and supersonic jet grazing and impingement. The type IV interaction produces the most significant increases in pressure and heat transfer and causes extremely high pressure and heat transfer rate gradients in highly localized regions where the interference pattern impinges on the surface. The extreme heat transfer rate gradient that occurs over these narrow impingement regions results in a large temperature gradient and attendant thermal stresses, which limit the duration of the structural component[9)]. However the previous work on these phenomena focused primarily on shock-shock interactions. This left a void for the designer of two-dimensional engine inlets that have the isentropic compression wave from the inlet compression surface intersecting a cylindrical leading edge oriented with its axis parallel to the plane of the isentropic compression wave. From a practical point of view, it is desirable for inlet designers to be able to predict these interactions and their effects. From an intellectual point of view, it is desirable to understand the interactions as fluid phenomena, and how they differ from the non-interacting cases to the shock interference cases.

This paper presents the first detailed pressure and heat transfer rate distributions on a cylinder resulting from a two dimensional shock wave interference pattern created by the isentropic compression wave intersecting the bow shock wave. The results were simulated by CFD++ software at a Mach number of 6. The position between the cylinder and the coalesced

point of the isentropic compression wave was varied to study the shock interference pattern and the heat transfer rate.

Simulation Model and Computation Method

Simulation Model

In this paper, our interest lies in the interference between the isentropic compression wave and the cowl bow shock wave. As a result, a sketch of the simulation model as shown in Fig. 1 was adopted. As shown in the upper view of Fig. 1, the impinging isentropic compression wave is drawn approaching from the lower, left quadrant of the flow field, with the flow approaching from the left. The cowl-lip is represented by a cylinder with radius equal to 3 mm. The flow passing beneath the cylinder enters the combustor, while the flow passing over the cylinder remains outside the engine. The turning angle of the isentropic surface is 12.5 degree, that is to say $\delta = 12.5^{\circ}$. The lower view of Fig. 1 is the enlarged intersecting section of an isentropic compression wave and the cowl bow shock wave. X and Y are the coordinates of the isentropic compression wave created by an isentropic wall coalescing point. The arc length of $\overset{\frown}{AB}$ demonstrates the strong portion of the bow shock wave. The arc length of $\overset{\frown}{CD}$ illustrates the intersection portion of the isentropic compression wave and the bow shock. θ is the angular position on cylinder, positive above undisturbed flow stagnation point.

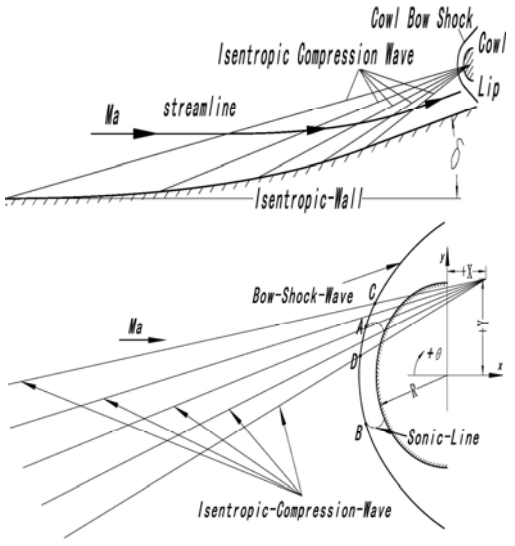

Fig. 1 Sketch of simulation model

Computation Method

The full Navier-Stokes equation is numerically solved by the CFD++ software. The convection terms of the governing equations are discretized with a second-order TVD method based on a new multi-dimensional interpolation framework, and Riemann solvers are used to define interface fluxes, based on local wave-model solutions. Multi-grid and dual time-step is used to accelerate convergence.

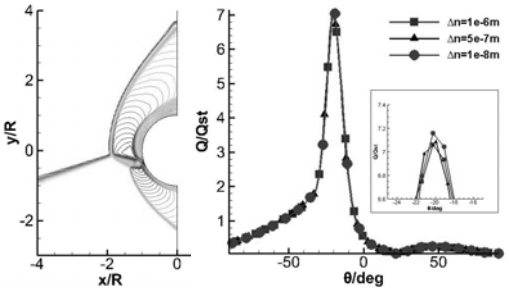

Fig. 2 R=3mm, X/R=-20/3, Ma=6, h=26km, $T_w = 294K, \delta = 12.5^{\circ}, Q_{st} = 2.35MW/m^2$, where the coalescing isentropic wave intersects the cowl bow shock. Left: Mach contour; Right: pressure and heat transfer rate distribution of the cowl wall.

The normal mesh spacing at the wall plays an important role in the accuracy of heat transfer rate[10-11]. Three different clustered meshes at the wall were used to predict heat transfer rate, as shown in Fig. 2 above. A supersonic jet is embedded in the subsonic region for Type IV shock-pattern and the region is very narrow. This need adequate meshes to capture the tiny structure. A supersonic jet and shear layer are found in the left view of Figure 2. The right of Figure 2 plots the heat transfer rate distribution of the cylinder wall which is normalized by the stagnation point pressure of the interference-free case in which the cylinder is embedded in the free stream condition. The horizontal coordinates are the circumferential angle, θ. Although the peak value has a slight discrepancy, the heat transfer rate distribution agrees very well for the first grid space at the wall of 1e-6, 5e-7, 1e-8 m, respectively. It is clear that the number of mesh reaches grid independence and the normal mesh spacing at the wall is enough to capture heat transfer rate.

Numerical Results and Discussion

Numerical results for laminar flows with free stream Mach number of 6 and the altitude of 26 kilometer are discussed below. The isentropic wall adopts an inviscid condition, while the cylindrical wall is assumed an isothermal-constant temperature of 294 K. A series of X and Y were examined to study the shock interference pattern and heat transfer rate. In this paper the result for X=0, 10, 20 with different Y is shown.

Shock Interference Pattern

It is clear that there are two extreme cases; the first is the nonuniform flow, in which the leading front of the cylinder is in the nonuniform flow, when the cylinder

is completely submerged in the isentropic wave and the second is equivalent to an oblique shock intersecting the cowl bow shock, which produces six types of shock interference patterns, when the coalesced isentropic wave interacts with the cowl shock wave. However the other cases are more practical and valuable for the designer of hypersonic inlet and are also our interest in this paper.

Firstly, we come to see the case that the isentropic wave before coalescing intersects the cowl bow shock but the intersection section of an isentropic compression wave and the bow shock related to the strong part of the cowl bow shock is very small, that is to say $\widehat{CD}$ / $\widehat{AB}$ is close to 0. In this case, the results for X/R=0 and Y/R=-1/2, 0, 1/3, 5/3 are shown in Fig. 3. From Mach contour in Fig. 3, it can be seen that shock interference pattern becomes different as the two interaction location changes. A late Type II interaction is shown in Fig. 3 (a) left. The Type III, IV shock interaction can be seen in Fig.3 (b), (d) left. The shear layer or supersonic jet can be clearly seen to impinge on the cowl-lip. Fig. 3 (d) left shows the shear surface passes well above the cylinder.

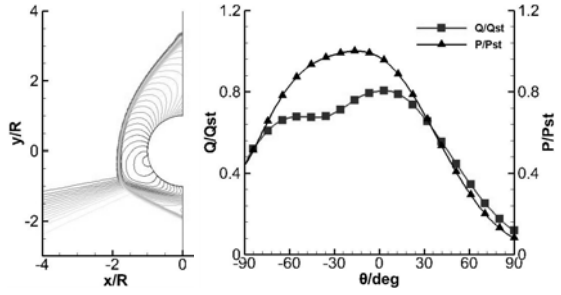

(a) Y/R=-1/2

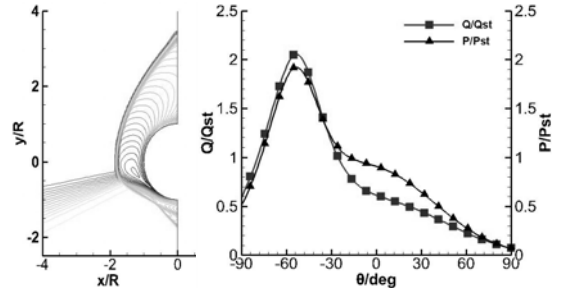

(b) Y/R=0

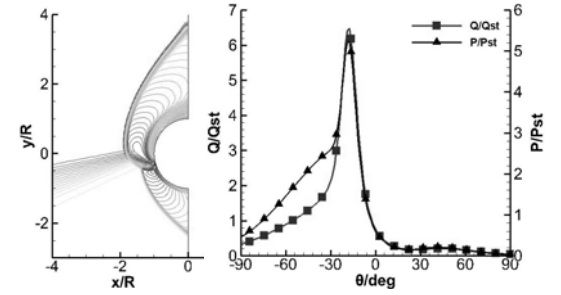

(c) Y/R=1/3

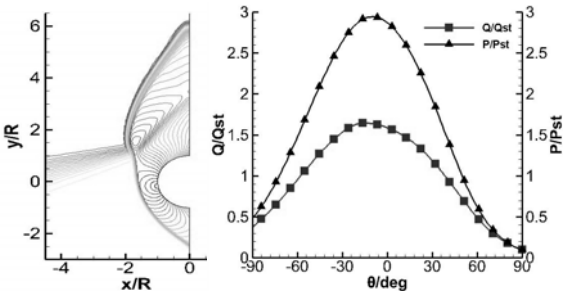

(d) Y/R=5/3

Fig. 3 R=3mm, X/R=0, Ma=6, h=26km, $T_w = 294K, \delta = 12.5^\circ, \widehat{CD} / \widehat{AB} \sim 0$, where the noncoalesced isentropic wave intersects the cowl bow shock. Left: Mach contour; Right: pressure and heat transfer rate distributions of the cowl wall.

Secondly, we come to see the case that the intersection portion of the isentropic compression wave and the bow shock is approximately equal to the strong part of the cowl bow shock. In this case, the results for X/R=10/3 and Y/R=1, 5/3, 7/3, 3 is shown in Fig. 4. From Fig. 4 left it can be found that no shock interference pattern is illustrated. As the two interaction location changes from the lower sonic line to the upper one, the flow structure has very little change. The shock wave is composed of three parts; the first part is the free stream as the condition of the formation of the bow shock, the second is the isentropic wave as the condition of the formation of the curved shock, the third is the air behind the isentropic wave as the condition of the formation of the bow shock.

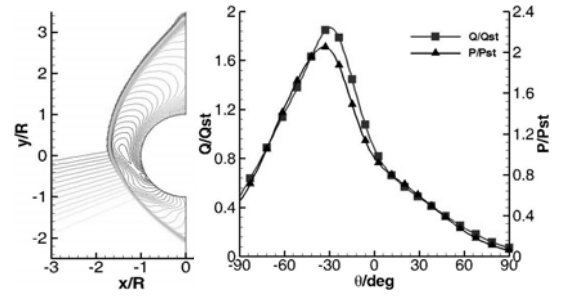

(a) Y/R=1

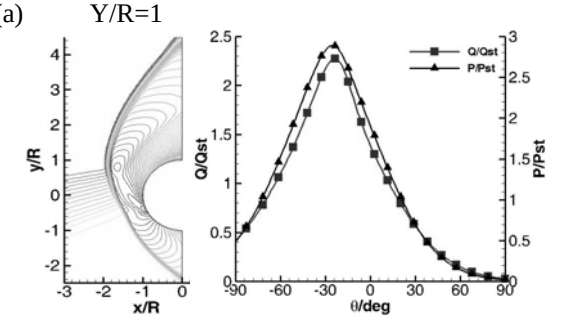

(b) Y/R=5/3

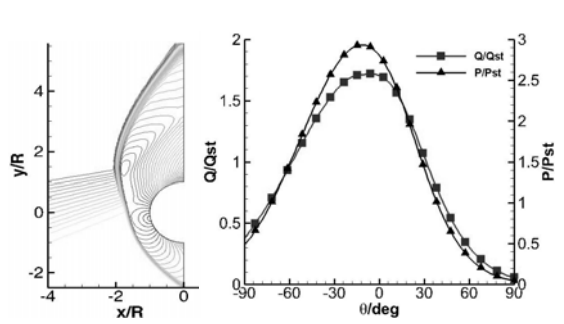

(c) Y/R=7/3

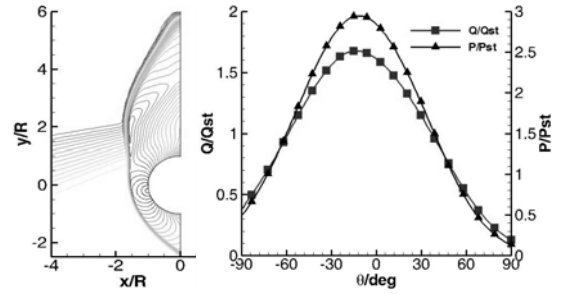

(d) Y/R=3

Fig. 4 R=3mm, X/R=10/3, Ma=6, h=26km, $T_w = 294K, \delta = 12.5^{\circ}, \overset{\frown}{CD} / \overset{\frown}{AB} \sim 1,$ where the noncoalesced isentropic wave intersects the cowl bow shock. Left: Mach contour; Right: pressure and heat transfer rate distributions of the cowl wall.

Thirdly, we come to see the case that the intersection portion of the isentropic compression wave and the bow shock is slightly greater than the strong portion of the cowl bow shock. In this case, the results for X/R=10/3 and Y/R=1, 5/3, 7/3, 3 is illustrated in Fig. 5. As can be seen that the shock structure is a little different from the one shown in Fig.4 Mach contour except for the transmitted nonuniform flow.

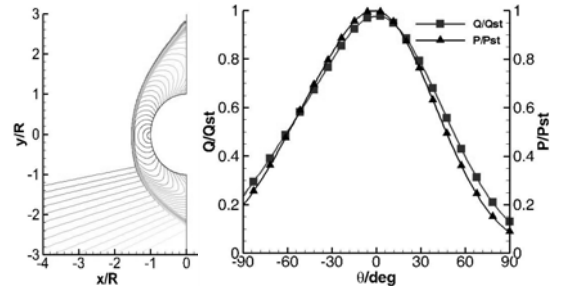

(a) Y/R=2/3

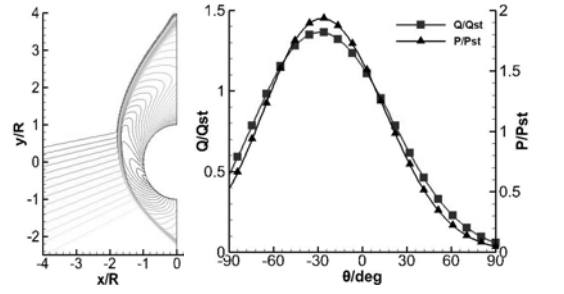

(b) Y/R=7/3

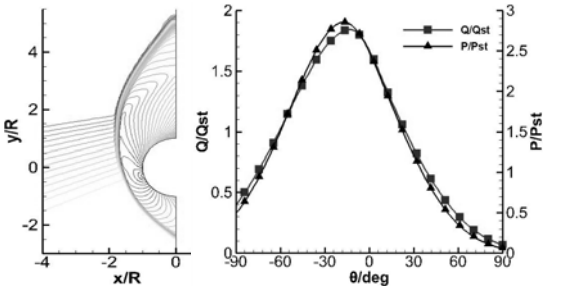

(c) Y/R=10/3

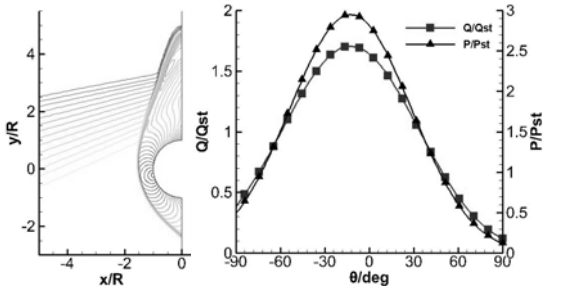

(d) Y/R=14/3

Fig. 5 R=3mm, X/R=20/3, Ma=6, h=26km, $T_w = 294K, \delta = 12.5^{\circ}, \overset{\frown}{CD} / \overset{\frown}{AB} > 1,$ where the noncoalesced isentropic wave intersects the cowl bow shock. Left: Mach contour; Right: pressure and heat transfer rate distributions of the cowl wall.

Comparing Figure 4 and 5 with Figure 3, it is demonstrated that the dispersion degree of the isentropic wave has an effect upon shock interaction. When the dispersion degree is very small, shock interference occurs because of pressure to match in the narrow region. There is a discontinuity from the pressure in front of the isentropic wave to that behind the isentropic wave. Pressure matching in the narrow region causes a transmitted shock wave and the shear layer which produce the shock interference pattern. When the intersection portion of the isentropic compression wave and the bow shock increases to some degree, there is enough region to finish pressure jump and non-shock-interference occurs. The

intersection is the curved shock at the nonuniform flow.

As mentioned above, it is revealed that whether shock interference pattern exists depends directly on the ratio of the intersection portion length of the isentropic compression wave and the bow shock to the strong part length of the cowl bow shock, or rather the ratio of $\overset{\frown}{CD}$ to $\overset{\frown}{AB}$. Shock interaction does not occur, when $\overset{\frown}{CD} / \overset{\frown}{AB}$ reaches the magnitude of 1.

Pressure and Heat Transfer Rate

The corresponding surface pressure and heat transfer rate distributions are shown in Figure 3, 4 and 5 right views. The pressures, normalized by the stagnation point pressure of the interference-free case, are presented versus the circumferential angle, θ, the same as heat transfer rate. The stagnation point pressure and heat flux of the interference-free case are 2.35 MW/m^2, 1.02 bar, respectively.

For shock interaction pattern occurs, the pressure and heat flux distribution are demonstrated in Figure 3 right view. From Figure 3 (a), as can be seen very little change in the pressure occurs for Type II from that of the non-interfering case. However the heat flux shows a double peak. The first peak results from the shear layer passing close to the body. The second is the free stagnation point. The maximum value is less than the stagnation point heat flux due to the increase of the shock standoff distance. From the pressure and heat flux distribution in Figure 3 (b), (c), (d), the pressure and heat flux ratio rapidly increases to reach a maximum for Type IV flow before dropping back to a lower level.

For no shock interaction pattern, the pressure and heat flux distribution are demonstrated in Figure 4 and 5 right views. From Figure 4 and 5 right views, it can be seen that the peak pressure and heat flux are larger than those of the stagnation point although there is no obvious shock interference pattern. As the two intersecting location moves from the low sonic line to the upper one, the peak pressure and heat flux also increases to reach a maximum before dropping back to lower level.

However the peak pressure and heat flux of non-shock-interaction-pattern differs from the one that shock interference pattern exists, as the intersecting position of the isentropic compression wave and the cowl shock moves from the low sonic line to the upper one. Figure 3 right view shows that the maximum of heat flux ratio is about seven, while Figure 4 right view illustrates that the maximum is approximately 2.5. Figure 5 right view presents that the maximum is approximately two. It can be concluded that the dispersion degree of the isentropic wave not only changes the shock interaction structure, but also decreases the maximum heat flux. When Type IV shock pattern cancels, the maximum heat transfer rate dramatically drops.

Conclusion

This paper presents the details of a numerical study of shock-on-isentropic-wave interference heating on a cylindrical leading edge representative of the cowl of a rectangular hypersonic engine inlet. The study was conducted at a condition of Mach number of 6, flight altitude of 26 kilometers. The model consisted of a 6-mm-diam cylinder and a turning angle 12.5-deg isentropic surface. The primary goal of this study was to obtain detailed surface pressure and heat transfer rate distributions along the circumference of the cylinder to fill a void in the data base for design.

This study has provided the first detailed heat transfer rate and pressure distributions on a cylinder for two-dimensional compression wave interference created by the isentropic wave intersecting the cylinder bow shock wave. Shock–interference-pattern, pressure and heat transfer rate which result from the noncoalesced isentropic compression wave intersecting the cowl bow shock depends directly on the ratio of the intersection portion length of the isentropic compression wave and the cowl shock to the strong part length of the cowl shock, that is to say $\overset{\frown}{CD} / \overset{\frown}{AB}$. When $\overset{\frown}{CD} / \overset{\frown}{AB}$ tends to the magnitude of zero as well as a noncoalesced isentropic compression wave intersecting cowl bow shock, Type IV shock pattern occurs and pressure, heat transfer rate dramatically amplifies. Otherwise, when $\overset{\frown}{CD} / \overset{\frown}{AB}$ draws near the magnitude of one, shock-pattern does not exist and the amplification of pressure, heat transfer rate decreases with $\overset{\frown}{CD} / \overset{\frown}{AB}$ increasing. The peak heat transfer rate and pressure to an engine cowl leading edge are minimized by the intersection portion between the isentropic compression wave and the cowl shock being approximately equal to the strong part of the cowl shock.

Acknowledgments

The authors wish to thank Tian WAN for his assistance in the algorithm of the numerical simulation and writing. The valuable suggestions of Xin LU and Fei LI are greatly appreciated.

References

1) John J B, Hypersonic Aerothermodynamics, American Institute of Aeronautics and Astronautics Inc. Washington, DC , 1994.
2) Edney, Barry, Anomalous Heat Transfer and Pressure Distributions on Blunt Bodies at Hypersonic speeds in the Presence of an Impinging Shock, FFA Rep. 115, Aeronaut. Res. Inst. Of Sweden, 1968.
3) Keyes, J.W. and F.D. Hains, Analytical and Experimental Studies of Shock Interference Heating in Supersonic Flows, NASA TN D-7139, May 1973.

4) Morris, Dana K. and Keyes, J. Wayne, Computer Programs for Predicting Supersonic and Hypersonic Interference Flow Field and Heating, NASA TM X-2725, May 1973.
5) Wieting, A. R. and Holden, M. S., Experimental Study of Shock Wave Interference Heating on a Cylindrical Leading Edge at Mach 6 and 8, AIAA Journal, vol.37, November 1989, pp. 1557-1565.
6) Wieting, A.R., Multiple Shock-Shock Interference on a Cylindrical Leading Edge, AIAA Journal of Propulsion and Power, Vol. 30, No.8,1992, pp. 2073-2079.
7) Frame, M. J. and Lewis, M. J., Analytical Solution of the Type IV Shock Interaction, AIAA Journal of Propulsion and Power, Vol. 13, September-October 1997, pp. 601-609.
8) Weixing Wang, Lvrong Xie and Rongwei Guo, Influence of Blunting Manner of the Lip Highlight of Hypersonic Inlet on the Aerothermodynamic Performance, AIAA 2011-2306.
9) Dechaumphai, P., Thornton, E. A., and Wieting, A. R., Flow -Thermal Structure Study of Aerodynamically Heated Leading Edges, Journal of Spacecraft and Rockets, Vol. 26, No. 4, July 1989, pp. 201-209.
10) Klopfer, G.H. and H.C. Yee, Viscous Hypersonic Shock-on-Shock Interaction on Blunt Cowl Lips, AIAA Paper 88-0233, AIAA 26th Aerospace Sciences Meeting, January 11-14,1988, Reno, Nevada.
11) YAN Chao, YU Jian-jun and LI Jun-zhe, Scheme effect and grid dependency in CFD computations of heat transfer, ACTA AERODYNAMICA SINICA, Vol.24 (2006), NO.1, pp.125-130.